Supplementary Information

Water and Solute Transport Governed by Tunable Pore Size Distributions in Nanoporous Graphene Membranes

Doojoon Jang[†], Juan-Carlos Idrobo[‡], Tahar Laoui[§], and Rohit Karnik[†,*]

[†]*Department of Mechanical Engineering, Massachusetts Institute of Technology, Cambridge, Massachusetts 02139, United States*

[‡]*Center for Nanophase Materials Sciences, Oak Ridge National Laboratory, Oak Ridge, Tennessee 37831, United States*

[§]*Department of Mechanical Engineering, King Fahd University of Petroleum and Minerals, Dhahran 31261, Saudi Arabia*

1. Pore Creation Procedure

Ion Bombardment Procedure

After interfacial polymerization to seal diffusive leakage across large graphene defects, ion bombardment was performed with gallium ions (Ga^+) to nucleate the defect sites for pore growth. With the fabricated membrane held to an SEM specimen holder by carbon tape, Helios Nanolab Dualbeam 600 was operated at voltage of 1 kV and nominal ion beam current of 6.7 nA to bombard 1.56 × 1.35 mm^2 (equivalent to 100× magnification) of graphene at 0° (vertical) or at 52° (inclined) incidence angle.[1] For vertical bombardment, dwell time of t μs per pixel and ion beam current of I nA resulted in the bombardment dose of $0.425 \cdot t \cdot I \times 10^{13}$ cm^{-2}. The ion beam shots were carried out over ~1 cm^2 graphene area, with predetermined spacing that avoids overlapping of adjacent shots and minimizes the non-bombarded gap between them. All the bombardment parameters and density attempted in this manuscript are summarized in Table S1.

Table S1. Ion bombardment parameters

Type	Beam current (nA)	Voltage (kV)	Dwell time (μs)	Incidence angle (°)	Bombardment density (cm^{-2})
Vertical / High	4.75-5.24	1	3	0	$6.06 - 6.68 \times 10^{13}$
Vertical / Low	4.71	1	1	0	2.00×10^{13}
Inclined / Low	1.71	8	1	52	0.55×10^{13}

Plasma Etching Procedure

Plasma etching was performed on a graphene membrane immediately following the ion bombardment to minimize contamination on graphene. Harrick Plasma's PCD-001 tabletop inductively coupled plasma cleaner was used to generate oxygen plasma for etching nucleated defect sites from bombardment. Prior to graphene etching, the plasma cleaner was operated for 300 s with its chamber empty to remove any impurities or residual polymer that could potentially contaminate the graphene membrane. The graphene membrane was placed on a clean glass slide with PCTE side down and its edge was fixed with Kapton tape. After the plasma cleaning with empty chamber, prepared graphene membrane was placed at the center of the RF solenoidal coils and the chamber was pumped down to ~200 mTorr. Oxygen was introduced into the chamber and pressure was stabilized at 390 mTorr. Plasma was generated at low RF power (~7.16 W) for desired etching time (10 - 90 s). The graphene membrane taken out of the plasma cleaner was immediately mounted on the diffusion cell for transport measurements to minimize any contamination from exposure to air.

2. Pore Diameter Measurements

Pore Diameter Estimation from STEM Images and van der Walls Diameter Correction

Pore diameters were estimated from annular dark field Scanning Transmission Electron Microscopy (STEM) images by looking for the areas with intensity below that of single layer graphene region, using the plot profile tool in ImageJ. Areas free from carbon electron cloud (as seen in the images) were selected with polygon selections tool and, from the measured pore area, effective pore diameter $d_{eff} = \sqrt{4Area_{pore}/\pi}$ was calculated as the diameter of a circle of the same area[1]. Pore density was estimated for each pore creation condition by dividing the pore counts with total inspected area (See Figure 3c,d).

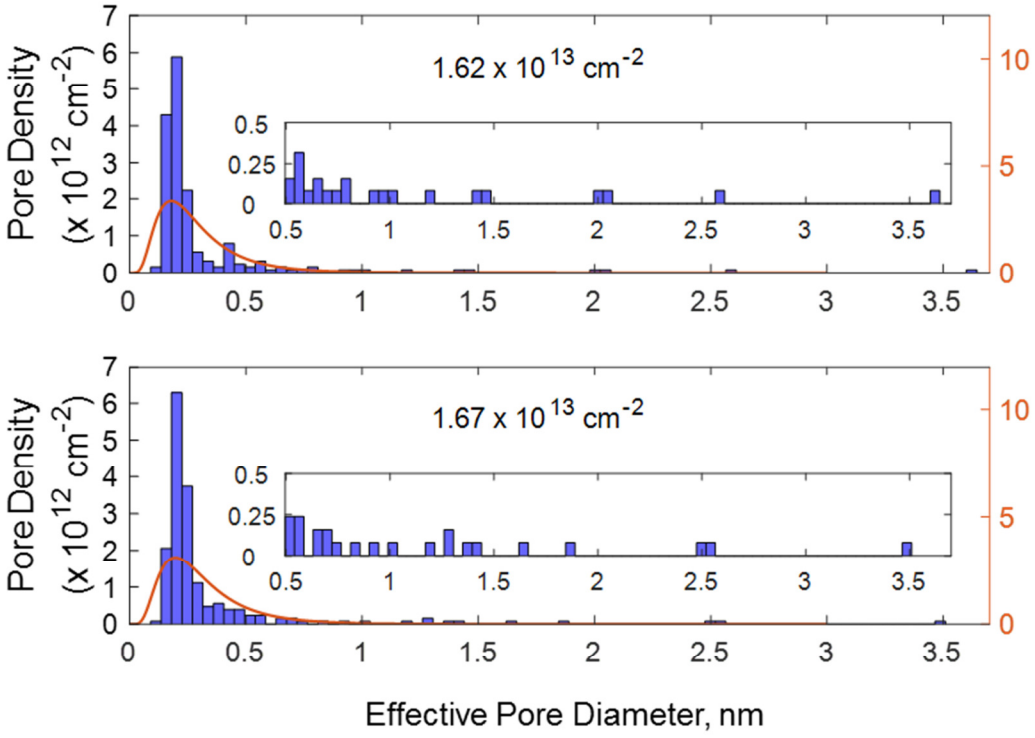

Figure S1. Direct transfer: pore diameter distribution from vertical/high bombardment followed by 30 s (top) and 50 s (bottom) of oxygen plasma etching. Inset: Magnified view for pores larger than 0.495 nm. Pore density (text) and lognormal probability density function (red) constructed for each condition are also considered.

However, the pore diameters measured from STEM images represent interaction of the atoms with high-energy electrons in the STEM and had to be adjusted to account for the effective open area accessible by traversing species in solution. Cohen-Tanugi et al. defined the pores in their molecular dynamics simulation as the contiguous area not obstructed by van der Walls spheres of atoms.[2] Since our pores were measured by obtaining the area not screened by electron clouds, the distance from the carbon atom's center to its electron cloud edge was acquired,[1] whose average from 10 measurements was 0.0695 nm. Twice the distance was added to the measured pore diameters from STEM images to obtain carbon center-to-center diameters. Then, the carbon atoms' van der Waals (vdw) diameter (0.34 nm) was subtracted to calculate the diameter of the open area not screened by carbon vdw spheres. This is equivalent to subtracting 0.2010 nm from the original measured pore diameters, or to shifting the entire pore size distribution to the left by the same distance. Upon this correction, some pores with negative diameters were considered unavailable for transport due to overlapping vdw spheres and thus were truncated.

Pore Diameter Distribution from Different Bombardment Parameters

To verify the effects of bombardment density and beam incidence angle, ion bombardment was carried out with different parameters on graphene transferred to TEM grids (direct transfer), followed by 30 s of plasma etching. As observed in transport measurements for 50 s plasma, lowering the vertical bombardment density to one-third (2×10^{13} cm^{-2}) significantly reduced the pore density at 30 s of plasma etching (See Figures S2 (left) and 2b); the nearly 90% reduction in pore density suggests that not all gallium ions bombarding graphene lattice are nucleating defects in one-to-one correspondence with carbon atoms. Inclined (52°) bombardment was performed at

one-tenth the density of vertical/high bombardment (see Table S1), leading to an order of magnitude drop in the resulting pore density. However, pores larger than 0.5 nm were observed after 30 s plasma despite the low bombardment dose. Inclined ion beam may be more effective in initiating defect sites than vertical bombardment, which will be helpful in introducing size-selective pores in graphene when combined with higher ion bombardment dose and short plasma etching time.

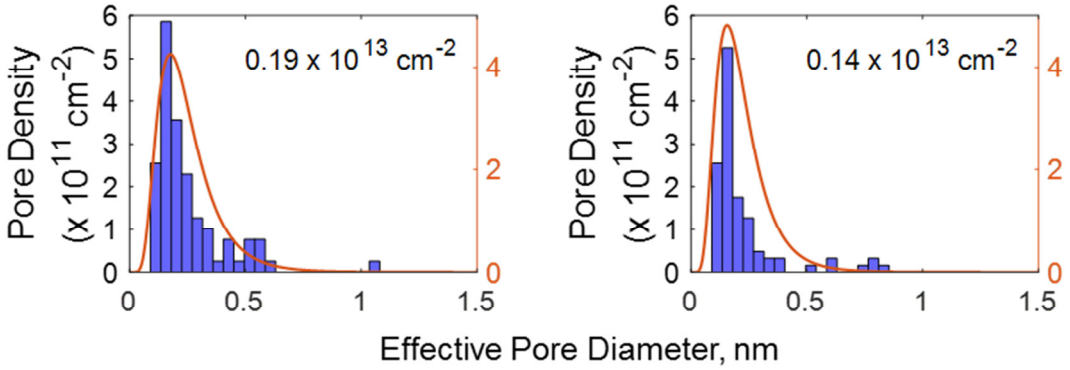

Figure S2. Direct transfer: pore diameter distribution from vertical/low (left) and inclined/low bombardment (right) followed by 30 s of oxygen plasma etching (see Table S1 for bombardment parameters and densities). Pore density (text) and lognormal probability density function (red) constructed for each condition are also considered. No pores beyond 1.2 nm were observed at either bombardment condition.

Since graphene membrane's performance is to be evaluated over the entire membrane area, the pore densities were estimated over total inspected area from STEM images. Nevertheless, it still remains unclear whether ion bombardment and plasma etching can create new pores underneath the contamination on graphene, and there is a possibility that small created pores were covered

by contamination attracted to graphene during transfer or STEM imaging. Therefore, dividing the pore counts by total area may underestimate the actual density of the pores that ion bombardment and plasma etching introduced to graphene. Table S2 provides pore densities acquired from both total area and contamination-free single-layer region only for different pore creation parameters. A fraction (~20%) of the imaged area comprised double-layer graphene, however, the number of pores in this region was negligible (<2%), and these pores were not included in the pore counts.

Table S2. Pore density from different ion bombardment and oxygen plasma etching parameters.

Transfer	Bombardment	Plasma etching (s)	Pore density (Based on total imaged area) (cm^{-2})	Pore density (Based on contamination-free single-layer area) (cm^{-2})	vdw-adjusted pore density (cm^{-2})
Direct	Vertical / High	10	0.39×10^{13}	1.44×10^{13}	0.21×10^{13}
	Vertical / High	30	1.59×10^{13}	7.92×10^{13}	0.82×10^{13}
	Vertical / High	50	1.64×10^{13}	5.56×10^{13}	1.12×10^{13}
	None	10	0.16×10^{13}	0.61×10^{13}	0.019×10^{13}
	None	30	0.45×10^{13}	1.64×10^{13}	0.30×10^{13}
	None	50	1.05×10^{13}	3.15×10^{13}	0.57×10^{13}
	Vertical / Low	30	0.19×10^{13}	1.42×10^{13}	0.097×10^{13}
	Inclined / Low	30	0.14×10^{13}	0.69×10^{13}	0.041×10^{13}
PCTE	Vertical / High	30	0.12×10^{13}	1.25×10^{13}	0.11×10^{13}
	Vertical / High	50	0.098×10^{13}	1.59×10^{13}	0.06×10^{13}

3. Transport Modeling

Modeling Assumptions

To analytically model water and solute transport across graphene nanopores, a system of monolayer graphene with nanopores on a single 200 nm diameter polycarbonate pore was

considered a simplified representation of the measured membranes. The pore size distributions obtained from STEM images were assumed to obtain the size distribution of pores over the 200 nm diameter graphene area over the PCTE pore, while maintaining the measured pore density (based on total inspected area).

Water and solute transport through the system was assumed to be at steady state and purely one directional along the pore axis. For simplicity, transport across the graphene pores was assumed to be entirely governed by steric size exclusion, without any electrostatic effects enhancing or hindering the transport. For both forward osmosis water transport and solute diffusion, solute concentrations were assumed uniform over each side of graphene, regardless of each individual pore size. Vigorous stirring during the experiments justified the assumption of almost identical concentration at graphene pore entrance to that of the bulk solution to neglect external concentration polarization at higher concentration side of the membrane.

Estimating the PCTE Area Fraction Sealed by Nylon Plugs

As the transport model neglects nylon plugs in its simple system, experimentally measured water and solute transport had to be recalculated over the PCTE pores free from nylon-6,6, when comparing with the model prediction. To estimate the area fraction of PCTE pores available for transport, Allura Red diffusion was measured across the graphene-PCTE membranes, by incrementally etching the graphene until the solute only sees transport resistance from the nylon plugs. As nylon-6,6 is not as susceptible to oxygen plasma as the graphene pores are, Allura Red diffusion eventually stops increasing with further etching, indicating that only the nylon plugs are offering resistance to diffusion of Allura Red.

Following every 15 s of plasma etching, Allura Red diffusion was measured across the graphene-PCTE membranes, and compared to the permeance of a bare PCTE membrane. Starting from 75 s of etching, Allura Red transport consistently increased with growing graphene pores and eventually plateaued after ~3 min of etching, after which the transport no longer increased with further etching. With the nylon plugs alone retarding the flow, the reduction in Allura Red diffusion was 43 and 60%, respectively, from each of two different measured membranes, suggesting that 40-57% of the PCTE pores are not sealed by nylon and available for transport. Accounting for the 10% porosity of PCTE membranes, the graphene area available for transport was assumed to be 4-5.7% of the total membrane area. When making a comparison with the model prediction, this range of the graphene area available for transport was used to estimate the water and solute flux per unit area of graphene, providing the upper and lower bounds in Figure 4b,c.

Solute Diffusive Transport

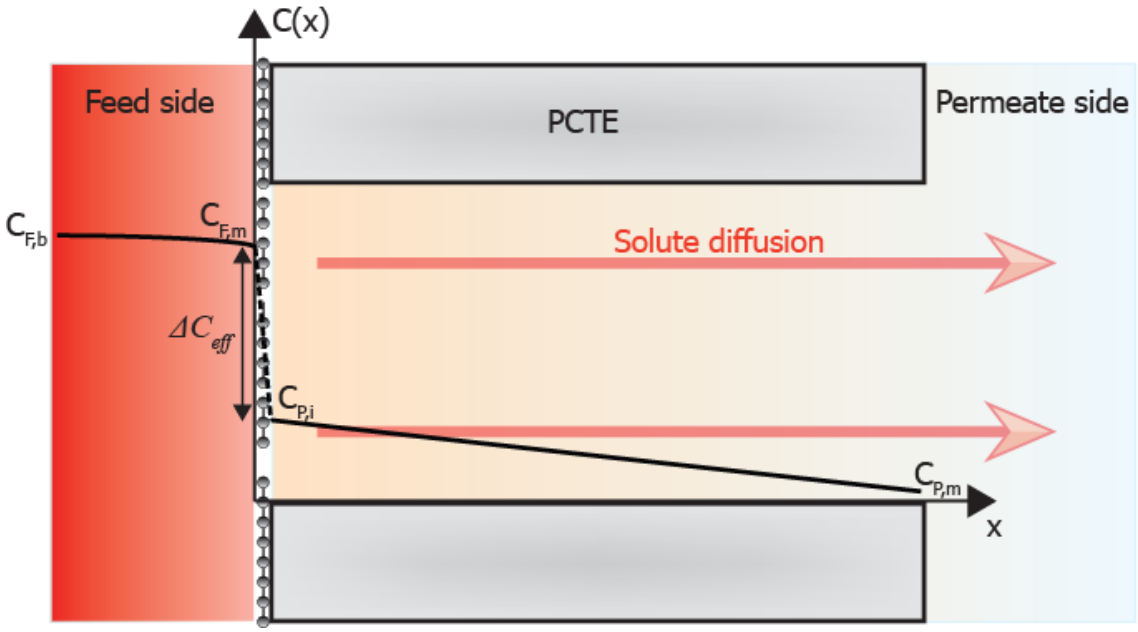

Figure S3. Schematic of solute diffusive transport across nanoporous graphene on a PCTE pore. Concentration drop across graphene indicates that effective concentration difference ΔC_{eff} is equal to or smaller than the concentration of feed solution $C_{F,m}$.

Solute diffusive transport was based on an assumption of steric hindrance and expected solute translocation only across the pores larger than KCl or Allura Red diameters, with $d_{pore} \geq 0.66$ nm and $d_{pore} \geq 1.0$ nm, respectively (All PCTE pore dimensions and solute properties for diffusion modeling are tabulated in Table S3). As shown in Figure S3, solute diffusion results in a rise in concentration at graphene-PCTE interface on permeate side, $C_{P,i}$, which consequently lowers net driving concentration difference across atomically thin graphene.

Solute molar flux (mol m^{-2} s^{-1}) across graphene pores r_i larger than the solute can be approximated with continuum diffusion theory as[3,4]

$$j_{diff}^{graphene} = D \sum_{r_i \geq r_{solute}} 2(r_i - r_{solute}) \frac{1}{A_{PCTE}} (C_{F,m} - C_{P,i}) \quad \text{(S1)}$$

where D is molecular diffusivity (m^2/s), A_{PCTE} is single PCTE pore area, and $C_{F,m}$ is solute concentration at graphene membrane's feed side.

Molar flux through the PCTE pore can be described by Fick's law as

$$j_{diff}^{PCTE} = -D \frac{\partial C}{\partial x} \quad \text{(S2)}$$

Since mass conservation requires flux across graphene pores to match PCTE pore flux,

$$D \sum_{r_i \geq r_{solute}} 2(r_i - r_{solute}) \frac{1}{A_{PCTE}} \left(C_{F,m} - C_{P,i}\right) = -D \frac{\partial C}{\partial x} \tag{S3}$$

The Nernst-Planck equation defines the solute transport within the PCTE pore as

$$\frac{\partial C}{\partial t} = D \frac{\partial^2 C}{\partial x^2} - \frac{\partial}{\partial x}(uC) \tag{S4}$$

where uC is convective flux of solutes. Assumption of steady state and $u = 0$ for diffusive transport can simplify eq S4 to

$$0 = D \frac{\partial^2 C}{\partial x^2} \tag{S5}$$

Applying boundary conditions at the PCTE pore entrance and exit as

$$C(x = 0) = C_{P,i}, C(x = L_{PCTE}) = C_{P,m} \tag{S6}$$

Equation (S5) can be solved to obtain a linear solute concentration profile $C(x)$ and its derivative $\frac{\partial C}{\partial x}$ as

$$C(x) = \frac{C_{P,m} - C_{P,i}}{L_{PCTE}} x + C_{P,i} \tag{S7}$$

$$\frac{\partial C}{\partial x} = \frac{C_{P,m} - C_{P,i}}{L_{PCTE}} \tag{S8}$$

From eqs S3 and S8, solute concentration at the interface $C_{P,i}$ can be obtained as

$$C_{P,i} = \frac{C_{F,m} \sum_{r_i \geq r_{solute}} 2(r_i - r_{solute}) + C_{P,m} \frac{A_{PCTE}}{L_{PCTE}}}{\sum_{r_i \geq r_{solute}} 2(r_i - r_{solute}) + \frac{A_{PCTE}}{L_{PCTE}}} \tag{S9}$$

From eqs S1 and S9, the membrane diffusive permeance (m s^{-1}) to KCl and Allura Red can be predicted for each pore size distribution as

$$K_{solute}^{membrane} = \frac{j_{diff}^{graphene}}{C_{F,m}} = D \sum_{r_i \geq r_{solute}} 2(r_i - r_{solute}) \frac{1}{A_{PCTE}} \frac{(C_{F,m} - C_{P,i})}{C_{F,m}} \quad \text{(S10)}$$

Table S3. PCTE and Solute properties for diffusion modeling

	Properties	Values
PCTE	Pore area A_{PCTE} (m^2)	3.1416×10^{-14}
	Pore length L_{PCTE} (m)	11.589×10^{-6}
KCl	Diameter d_{solute} (nm)	0.66
	Diffusivity D (m^2/s)	1.852×10^{-9}
	Feed solution concentration $C_{F,m}$ (mmol/L)	500
Allura Red	Diameter d_{solute} (nm)	1.0
	Diffusivity D (m^2/s)	0.36×10^{-9}
	Feed solution concentration $C_{F,m}$ (mmol/L)	1.2

Forward Osmosis Water Transport

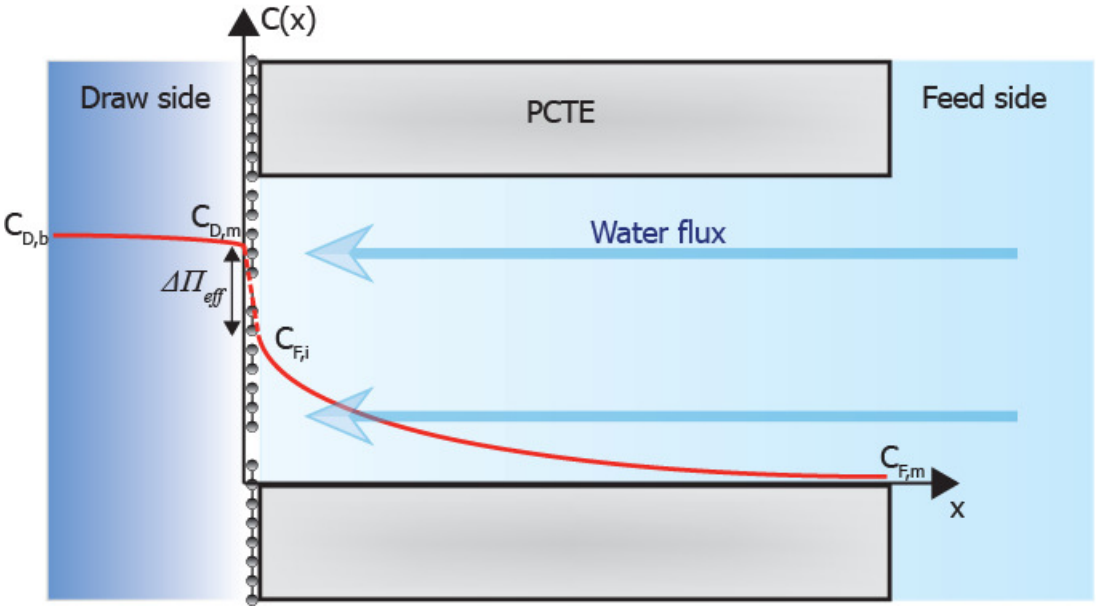

Figure S4. Schematic of water transport under forward osmosis across nanoporous graphene on a PCTE pore. Concentration drop across graphene indicates that effective osmotic pressure difference $\Delta\Pi_{eff}$ is equal to or smaller than the osmotic pressure of draw solution $\Pi_{D,m}$.

Water transport model under forward osmosis was also based on an assumption of steric hindrance defining water permeable pores to be in the range between water and glycerol ethoxylate molecule diameters (0.275 nm ≤ d_{pore} ≤ 1.2 nm), where osmotic pressure gradient can be established. (All water and glycerol ethoxylate properties for water transport modeling are tabulated in Table S4.)

No-slip hydrodynamics through nanopores in a two dimensional plane was used to theoretically estimate water flux across permeable pores assuming constant viscosity as[5]

$$u = K_{water}^{graphene}\Delta\Pi = \frac{\pi \sum_{r_{water}\le r_i\le r_{solute}} {r_i}^4}{\mu\left(3\pi \sum_{r_{water}\le r_i\le r_{solute}} r_i + 8L_{graphene}\right)} \frac{1}{A_{PCTE}}\, \Pi_{D,m} \qquad \text{(S11)}$$

where μ is dynamic viscosity of water, $L_{graphene}$ denotes graphene thickness (0.5354 nm), and $\Pi_{D,m}$ is osmotic pressure at graphene membrane's draw side. Our model does not take hydrodynamic interaction among adjacent water permeable pores into consideration since the large spacing between pores relative to their diameters makes it almost negligible.[6]

However, the presence of pores larger than glycerol ethoxylate presents diffusive leakage pathways for the draw solutes, leading to concentrative internal concentration polarization within PCTE pores, as shown in Figure S4. With increased solute concentration at graphene-PCTE interface on feed side $C_{F,i}$, the compromised effective osmotic pressure difference $\Delta\Pi_{eff} = \Pi_{D,m} - \Pi_{F,i}$ driving water transport requires eq S11 to be rewritten as

$$u = K_{water}^{graphene}\left(\Pi_{D,m} - \Pi_{F,i}\right) = \frac{\pi \sum_{r_{water}\le r_i\le r_{solute}} {r_i}^4}{\mu\left(3\pi \sum_{r_{water}\le r_i\le r_{solute}} r_i + 8L_{graphene}\right)} \frac{\left(\Pi_{D,m} - f\left(C_{F,i}\right)\right)}{A_{PCTE}} \qquad \text{(S12)}$$

where $f(C)$ is the relation defining osmotic pressure Π (Pa) of aqueous glycerol ethoxylate draw solution with osmolyte concentration C (wt%) as[1,7]

$$\Pi = f(C) = 10^{4.87+0.8C^{0.34}} \cdot 9.8692 \cdot 10^{-7} \cdot 101325 \quad \text{(S13)}$$

A set of continuity and Nernst-Planck equations was constructed to model the diffusive and convective draw solute transport and to solve for its concentration at graphene-PCTE interface $C_{F,i}$. Draw solute molar flux across graphene pores r_i larger than glycerol ethoxylate is modeled using continuum diffusion theory as[3,4]

$$j_{diff}^{graphene} = D \sum_{r_i \geq r_{glycerol}} 2(r_i - r_{glycerol}) \frac{1}{A_{PCTE}} (C_{D,m} - C_{F,i}) = K_{diff}^{graphene} (C_{D,m} - C_{F,i}) \quad \text{(S14)}$$

where D is glycerol ethoxylate molecular diffusivity, K_{diff} is diffusive permeance (m s^{-1}) of graphene, and $C_{D,m}$ is solute concentration at graphene membrane's draw side.

Molar flux across the PCTE pore has both diffusive and convective parts, which are expressed as

$$j_{total}^{PCTE} = j_{diff}^{PCTE} + j_{conv}^{PCTE} = -D \frac{\partial C}{\partial x} + uC(x) \quad \text{(S15)}$$

From continuity, molar flux through graphene and PCTE should be equal, requiring

$$K_{diff}^{graphene} (C_{D,m} - C_{F,i}) = -D \frac{\partial C}{\partial x} + uC(x) \quad \text{(S16)}$$

Assuming steady state forward osmosis with constant water flux $u \neq u(x)$, the Nernst-Planck equation in eq S4 can be also established for the draw solutes and simplified to the following form with boundary conditions at the PCTE pore entrance and exit as

$$0 = D \frac{\partial^2 C}{\partial x^2} - u \frac{\partial C}{\partial x} \quad \text{(S17)}$$

$$C(x = 0) = C_{F,i}, C(x = L_{PCTE}) = C_{F,m} \quad \text{(S18)}$$

Then, the draw solute concentration profile and its derivative can be expressed as

$$C(x) = \frac{\left(C_{F,i} - C_{F,m}\right)}{1 - e^{\frac{u}{D}L_{PCTE}}} e^{\frac{u}{D}x} + \frac{\left(C_{F,m} - C_{F,i}e^{\frac{u}{D}L_{PCTE}}\right)}{1 - e^{\frac{u}{D}L_{PCTE}}} \quad \text{(S19)}$$

$$\frac{\partial C}{\partial x} = \frac{u}{D}\frac{\left(C_{F,i} - C_{F,m}\right)}{1 - e^{\frac{u}{D}L_{PCTE}}} e^{\frac{u}{D}x} \quad \text{(S20)}$$

From eqs S16, S19, and S20,

$$K_{diff}^{graphene}\left(C_{D,m} - C_{F,i}\right) = -D\frac{\partial C}{\partial x} + uC(x) = u\frac{\left(C_{F,m} - C_{F,i}e^{\frac{u}{D}L_{PCTE}}\right)}{1 - e^{\frac{u}{D}L_{PCTE}}} \quad \text{(S21)}$$

The draw solute concentration at graphene-PCTE interface can be summarized as

$$C_{F,i} = \frac{K_{diff}^{graphene}C_{D,m}\left(1 - e^{\frac{u}{D}L_{PCTE}}\right) - uC_{F,m}}{K_{diff}^{graphene}\left(1 - e^{\frac{u}{D}L_{PCTE}}\right) - ue^{\frac{u}{D}L_{PCTE}}}, \quad K_{diff}^{graphene} = \frac{D}{A_{PCTE}}\sum_{r_i \geq r_{gly}} 2\left(r_i - r_{glycerol}\right) \quad \text{(S22)}$$

For each pore size distribution, a set of eqs S12 and S22 are solved to acquire water flux u and interface concentration $C_{F,i}$. Then, the membrane permeance to water can be defined as

$$K_{water}^{membrane} = \frac{u}{\Pi_{D,m}} = \frac{\pi\sum_{r_{water} \leq r_i \leq r_{solute}} {r_i}^4}{\mu\left(3\pi\sum_{r_{water} \leq r_i \leq r_{solute}} r_i + 8L_{graphene}\right)}\frac{1}{A_{PCTE}}\frac{\left(\Pi_{D,m} - f\left(C_{F,i}\right)\right)}{\Pi_{D,m}} \quad \text{(S23)}$$

Table S4. Water and glycerol ethoxylate properties for water transport modeling

	Properties	Values
Water	Diameter d_{water} (nm)	0.275
	Water viscosity μ (Pa-s)	8.90×10^{-4}
Glycerol Ethoxylate	Average molecular weight M_n	~ 1,000
	Diameter d_{solute} (nm)	~ 1.2
	Diffusivity D (m^2/s)	0.33×10^{-9}
	Draw solution concentration $C_{D,m}$ (wt%)	26.4671
	Draw solution osmotic pressure $\Pi_{D,m}$ (atm)	22.557

Internal Concentration Polarization with Different Draw Solution Concentrations

The developed model for water transport under forward osmosis takes into account the roles of both water permeable and draw solute permeable pores in permitting water flux and lowering effective driving pressure difference across graphene, respectively. Larger graphene pores diminish the osmotic pressure difference, while pores smaller than draw solutes, in theory, should maintain the applied osmotic pressure difference. This trend arising from internal concentration polarization is prevalent in typical pressure range used in RO, and becomes more significant at higher draw solution osmotic pressure (Figure S5). Bombarded graphene etched with 10 s plasma for direct transfer and 30 s for PCTE transfer had no pores larger than glycerol ethoxylate and experienced no reduction in the osmotic pressure difference at virtually all range. However, all the other measured pore size distributions contained pores larger than the draw solute and exhibited intensifying concentration polarization of the leaked draw solute within the PCTE pores with increasing draw solution osmotic pressure due to enhanced water flux.

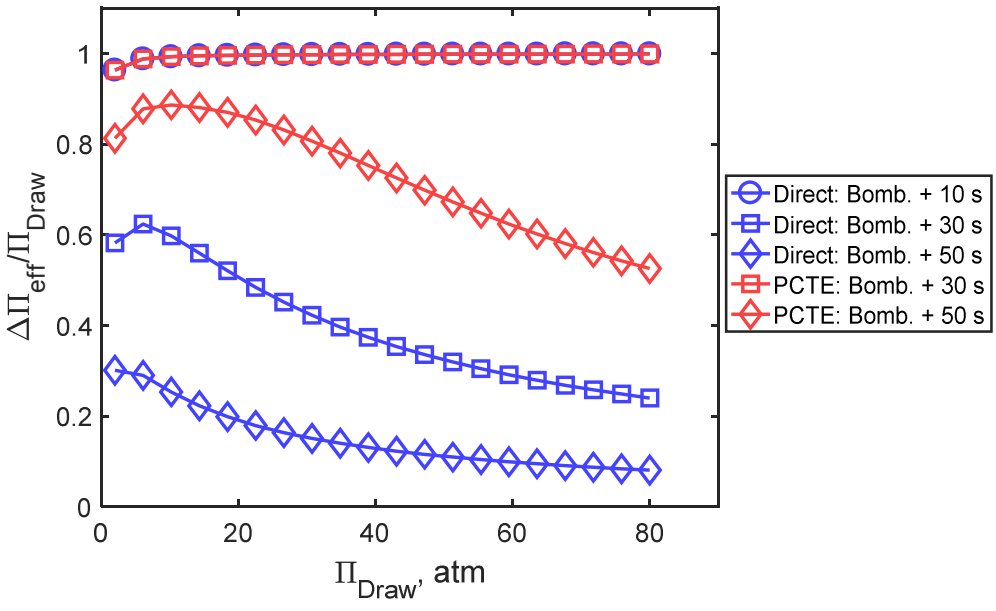

Figure S5. Variation of concentration polarization, shown as the effective osmotic pressure difference across graphene normalized by the draw solution osmotic pressure, with the draw solution osmotic pressure. The non-monotonic behavior at low osmotic pressure results from the assumption of diffusion in the dilute limit in the model, in conjunction with a highly non-linear dependence of osmotic pressure on concentration.

Effects of Heterogeneous Pores on Water and KCl Transport at Short Plasma Etching Time

The measured KCl diffusion suddenly increased, by a factor of three, from 20 to 30 s of plasma etching time (see Figure 2c). On the other hand, the steepest increase in osmotically driven water transport was observed at later etching time, from 30 to 40 s, despite the smaller size of water molecules than hydrated K^+ or Cl^- ions. It was hypothesized that the emergence of large, heterogeneous pores from plasma etching may be responsible for the different trends in KCl and water transport. To understand how the presence of a few large pores affects the transport, a very low density (1.6 - 8.0 × 10^{10} cm^{-2}) of heterogeneous pores with vdw-adjusted diameter 1.249 nm were added to the pore diameter distribution of the vertically bombarded 'direct transfer' sample at 10 s of etching. Pores larger than draw solutes do not participate in water flux, but only allow for the solutes to diffuse across, aggravating the concentrative internal concentration polarization. Our model predicts decreasing membrane permeance to water with increasing number of heterogeneous pores (Figure S6). On the other hand, the heterogeneity will only enhance the diffusive membrane permeance to solute $K_{solute}^{membrane}$ by providing more diffusive pathways, overwhelming the reduction in driving concentration difference (see eq S10). With the addition of the large pores, KCl transport increases by ~80%, exhibiting the opposite trend to water

transport under forward osmosis. If a few large pores smaller than the draw solutes are further added, the resultant increase in KCl transport will be greater than that of water, similar to the observed trends from transport measurements in 20 and 30 s of plasma etching.

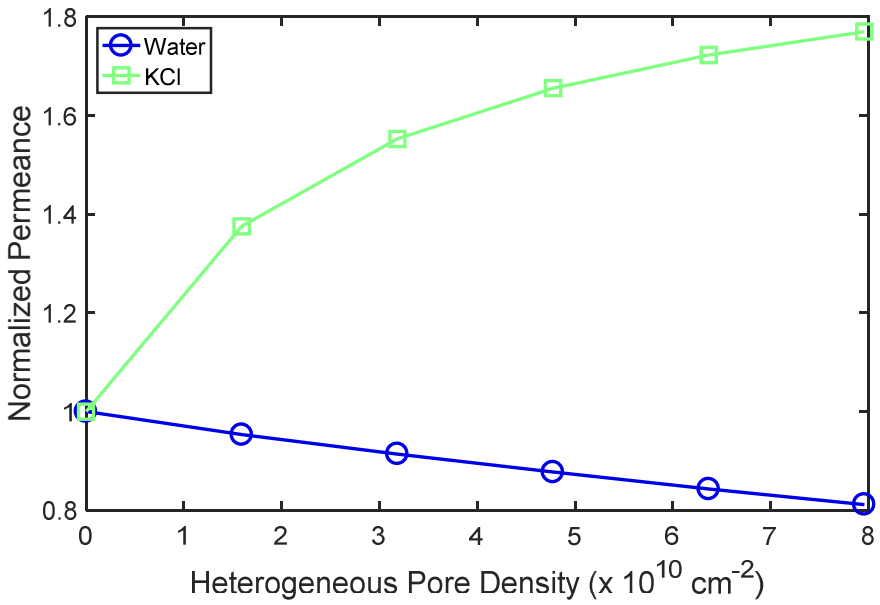

Figure S6. Normalized membrane permeance to water and KCl as a function of the density of additional heterogeneous pores.

4. Water Permeation Coefficient Calculation

Weighted Pore Diameter and Water Permeation Coefficient per Single Pore

Weighted diameter is defined as an approximate diameter of uniform pores that will allow for the same water permeance as the original pore size distribution. After taking vdw diameter of carbon atoms into account, water permeable pore size distribution and density from STEM images were used to calculate the weighted pore diameter of each pore creation condition for both direct and PCTE transfer. Since water flow rate is expected to have an approximately quadratic dependence

on radius for small pores (when pore size is smaller than pore length), the weighted pore diameter for each distribution was estimated as

$$r_{weighted} = \left(\sum_{r_{water} \le r_i \le r_{solute}} \frac{r_i^4}{N_{r_{water} \le r_i \le r_{solute}}} \right)^{1/4} \quad \text{(S24)}$$

where N is the number of the water permeable pores.

Water permeance from the forward osmosis experiments or no-slip hydrodynamics without concentration polarization was converted to find water permeation coefficient (ns^{-1} pa^{-1}) per single weighted pore and to make comparison with molecular dynamics simulations' predictions[1]. From experimental or theoretical permeance K_{water}, water permeation coefficient p can be calculated as

$$p = K_{water} \frac{\rho_{water}}{M_{water}} \frac{N_A}{n_{water}} \quad \text{(S25)}$$

where ρ_{water} is density of water (998.57 kg/m^3), M_{water} denotes molar mass of water (18.01528 g/mol), N_A represents Avogadro's number (6.022×10^{23} mol^{-1}) and n_{water} is density of water permeable pores for each distribution.

The lower limits of the experimental water permeation coefficients were acquired using the pore size distribution from 'direct transfer', assuming that 57% of PCTE pores are unsealed by nylon plugs and thus available for water transport. The experimental water permeance was recalculated over the nylon-free area and the permeation coefficient was estimated using the water permeable pore density from 'direct transfer'. On the other hand, the upper bounds were estimated from 'PCTE transfer', with 40% of PCTE pores assumed to be unplugged by the nylon.

5. Supporting Information References

(1) O'Hern, S. C.; Jang, D.; Bose, S.; Idrobo, J.-C.; Song, Y.; Laoui, T.; Kong, J.; Karnik, R. Nanofiltration across Defect-Sealed Nanoporous Monolayer Graphene. *Nano Lett.* **2015**, *15*, 3254–3260.

(2) Cohen-Tanugi, D.; Grossman, J. C. Water Desalination across Nanoporous Graphene. *Nano Lett.* **2012**, *12*, 3602–3608.

(3) O'Hern, S. C.; Stewart, C. A.; Boutilier, M. S. H.; Idrobo, J.-C.; Bhaviripudi, S.; Das, S. K.; Kong, J.; Laoui, T.; Atieh, M.; Karnik, R. Selective Molecular Transport through Intrinsic Defects in a Single Layer of CVD Graphene. *ACS Nano* **2012**, *6*, 10130–10138.

(4) O'Hern, S. C.; Boutilier, M. S. H.; Idrobo, J.-C.; Song, Y.; Kong, J.; Laoui, T.; Atieh, M.; Karnik, R. Selective Ionic Transport through Tunable Subnanometer Pores in Single-Layer Graphene Membranes. *Nano Lett.* **2014**, *14*, 1234–1241.

(5) Suk, M. E.; Aluru, N. R. Molecular and Continuum Hydrodynamics in Graphene Nanopores. *RSC Adv.* **2013**, *3*, 9365-9372.

(6) Jensen, K. H.; Valente, A. X. C. N.; Stone, H. A. Flow Rate through Microfilters: Influence of the Pore Size Distribution, Hydrodynamic Interactions, Wall Slip, and Inertia. *Phys. Fluids* **2014**, *26*, 52004.

(7) R. P. Rand. Osmotic Pressure Data: 1000 Da Polyethylene Glycol http://www.brocku.ca/researchers/peter_rand/osmotic/osfile.html (accessed Jan 3, 2016).